Framework Design of an Anterior Fiber-Reinforced Hybrid Composite Fixed Partial Denture: A 3D Finite Element Study

Daiichiro Yokoyama, DDS, PhD[a]/Akikazu Shinya, DDS, PhD[a,b]/Lippo V.J. Lassila, DDS, MSc Eng[c]/Harunori Gomi, DDS, PhD[d]/Yuji Nakasone, MSc Eng, PhD[e]/Pekka K. Vallittu, DDS, PhD, CDT[f]/Akiyoshi Shinya, DDS, PhD[g]

Purpose: The aim of this study was to investigate the optimal design of a fiber-reinforced composite (FRC) framework to obtain the maximum reinforcement for fixed partial dentures (FPDs) under three different loading conditions using three-dimensional finite element (FE) analysis. ***Materials and Methods:*** A three-unit FPD replacing the maxillary right lateral incisor was constructed using FE analysis software (ANSYS 10.0, ANSYS). A fiber framework of the pontic was designed with three variations: with the main framework curved labially (FRC1), located in the center (FRC2), or curved lingually (FRC3). Each framework was compared with a hybrid composite FPD without any fiber reinforcement (C-FPD). A lateral load was applied to the three different loading points of the pontic 0 mm, 3 mm, and 6 mm from the incisal edge, each representing loading conditions 1, 2, and 3, respectively. ***Results:*** Localized high stress concentration was observed around the connectors under all loading conditions. In all FRC-FPD models, the FRC framework showed stress-bearing capacity for the FPD. The highest stress reduction ratio under all loading conditions was obtained using the FRC1 model. The FRC1 framework also best reduced displacement of the framework. ***Conclusion:*** This study suggests that the optimum design of an FRC framework is to labially curve the FRC of the main framework at the region of the pontic. *Int J Prosthodont 2009;22:405–412.*

Hybrid composite resins are clinically applicable to inlays, onlays, and crowns. The recent evolution of fiber-reinforced composite (FRC) resins has created a new era in metal-free, esthetic dentistry.[1–4]

[a]*Lecturer, Department of Crown and Bridge, School of Life Dentistry at Tokyo, The Nippon Dental University, Tokyo, Japan.*
[b]*Visiting Research Scientist, Department of Prosthetic Dentistry and Biomaterials Science, Institute of Dentistry, University of Turku, Turku, Finland.*
[c]*Research Associate, Department of Prosthetic Dentistry and Biomaterials Science, Institute of Dentistry, University of Turku, Turku, Finland.*
[d]*Assistant Professor, Department of Crown and Bridge, School of Life Dentistry at Tokyo, The Nippon Dental University, Tokyo, Japan.*
[e]*Professor, Computational Solid Mechanics Laboratory, Department of Mechanical Engineering, Science University of Tokyo, Tokyo, Japan.*
[f]*Professor, Department of Prosthetic Dentistry and Biomaterials Science, Institute of Dentistry, University of Turku, Turku, Finland.*
[g]*Professor, Department of Crown and Bridge, School of Life Dentistry at Tokyo, The Nippon Dental University, Tokyo, Japan.*

Correspondence to: *Dr Akikazu Shinya, Department of Biomaterials Science, Institute of Dentistry, University of Turku and BioCity Turku Biomaterials Research Program, Lemminkäisenkatu 2, FI-20520 Turku, Finland. Fax: +358 2 333 8390. Email: akikazu.shinya@utu.fi*

The clinical applications of FRCs have been investigated from different points of view in terms of the quantity of fibers for reinforcement, matrix coupling, biocompatibility, fatigue properties, the type of fiber, and bending strength.[5–18] Designs for a fiber framework for posterior fixed partial dentures (FPDs) have been extensively investigated using finite element (FE) analysis, resulting in the notion that the reinforcement effects differ and depend on the position of the fiber framework.[19,20] The framework structure of an FRC-FPD consists of *(1)* a main framework that supports the FPD against vertical loads; *(2)* bonding wings or full-coverage crowns on the abutments, which increase resistance against dislodgement; and *(3)* additional fibers placed to support the pontic against delamination. In the anterior region, curving the main framework labially could provide an alternative to the use of additional fibers.

Anterior and posterior teeth play different roles in masticatory movement. While chewing, the maxillary and mandibular anterior teeth come into contact in the edge-to-edge occlusal position, after a sliding movement on the lingual surface, and then progress into the intercuspal position. Prosthetic appliances placed in the anterior region are subjected to the influence of the

© 2009 BY QUINTESSENCE PUBLISHING CO, INC. PRINTING OF THIS DOCUMENT IS RESTRICTED TO PERSONAL USE ONLY. NO PART OF THIS ARTICLE MAY BE REPRODUCED OR TRANSMITTED IN ANY FORM WITHOUT WRITTEN PERMISSION FROM THE PUBLISHER.

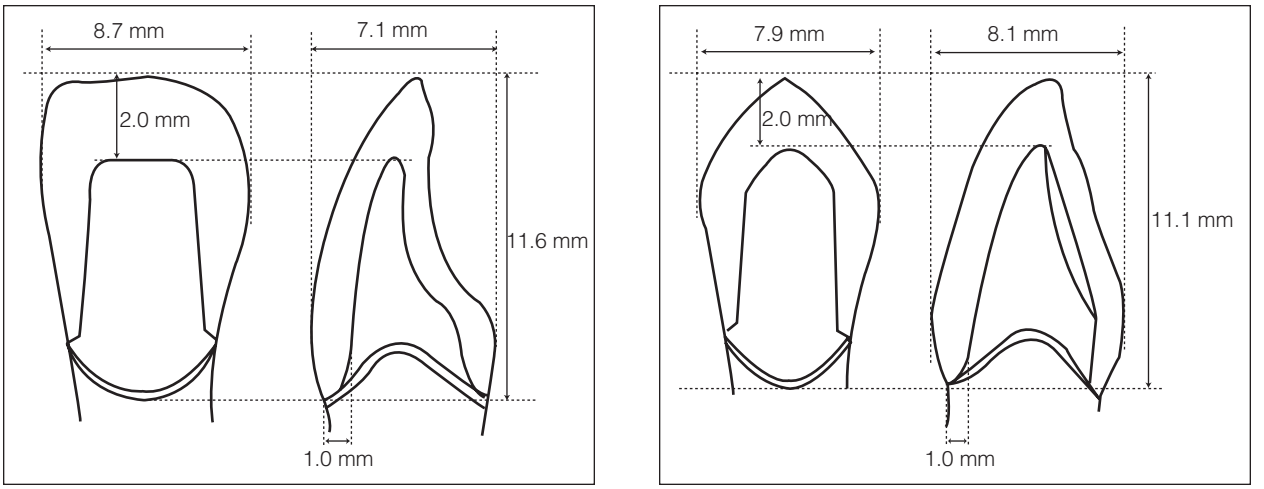

Fig 1 Preparation design and dimensions of the abutment teeth. *(left)* Maxillary right central incisor; *(right)* maxillary right canine.

diverse occlusal contacts of maxillary and mandibular teeth, as well as to the occlusal force of the masticatory movement. Due to the different crown contours and loading conditions, the mechanical behavior of FRC-FPDs in the anterior region is quite different from that of the posterior region. Consequently, it is indispensable to elucidate the relationship between the position of fiber placement and the stress reduction ratio.

The present study investigated the optimal design of an FRC framework to obtain the maximum reinforcement for anterior FPDs. FRC frameworks were designed using three different variations in the pontic. The results were compared with the control, a hybrid composite FPD without any fiber reinforcement, using the three-dimensional (3D) FE method.

Materials and Methods

Preparation of the C-FPD FE Model

To create an FE model, a three-unit FPD replica of the maxillary right central incisor to maxillary right canine replacing the maxillary right lateral incisor was fabricated. The replica (D51-SC41, Nisshin) was made in accordance with the *Textbook of Dental Anatomy*[21] and the following anatomic measurements were used: mesiodistal distance of the FPD (23.5 mm) and crown length (11.0 mm). Considering the esthetic and physiologic requirements, a modified ridge-lap pontic design was used for the missing maxillary right lateral incisor. Cross-sectional morphology of an FPD connector was created referencing that of a ceramometal FPD. Preparation designs are shown in Fig 1.

A 1-mm circumferential reduction shoulder preparation and a 2-mm incisal reduction were prepared for an assumed jacket crown. Because cementum, periodontal regiment, and alveolar bone were thought to have only a slight influence on the magnitude and distribution of stresses, they were ignored and a complete FPD-abutment interface was established.[22–25] A replica was measured at 0.25-mm intervals using a 3D dental computer-aided design unit (Dental Cadim, ADVANCE) and the contact scanning method.[26] The preprocessor of an FE analysis program (ANSYS 10.0, ANSYS) generated point clouds describing the replica surface, which were used as input data for the FE model (Fig 2).

Preparation of the FRC-FPD FE Models

The FRC-FPD FE models were composed of the C-FPD with an FRC framework (3.0 mm wide by 1.0 mm high). The mesiodistal distance of the FRC framework was constructed to extend from the mesial side of the central incisor distally to the canine, covering both of the abutment teeth. Figure 3 demonstrates three different curvatures of the FRC framework in the pontic of the FE model (ie, labially, at the center, and lingually). The distance between the labial side of mesiodistal center of the pontic and the fiber framework was defined as A. The radius of curvature (r) varied with the value of A and both connectors. Accordingly, three different FRC-FPD FE models were constructed depending on the radius of curvature obtained: FRC1 (A = 0.5 mm, r = 3.5 mm, labial side, curved line), FRC2 (A = 1.5 mm, r = 5.0 mm, at the center, curved line), and FRC3 (A = 3.0 mm, r = 0.0 mm, lingual side, straight line) (Fig 3).

Material Properties

The properties of the materials used for this FE analysis are listed in Table 1. Most of these values were determined according to previous literature surveys.[16,20–23] A hybrid composite with isotropic material properties

© 2009 BY QUINTESSENCE PUBLISHING CO, INC. PRINTING OF THIS DOCUMENT IS RESTRICTED TO PERSONAL USE ONLY. NO PART OF THIS ARTICLE MAY BE REPRODUCED OR TRANSMITTED IN ANY FORM WITHOUT WRITTEN PERMISSION FROM THE PUBLISHER.

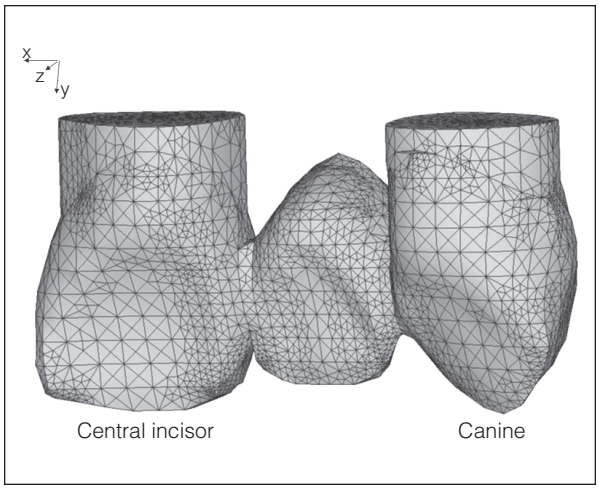

Fig 2 External form of the FPD FE model (lingual view).

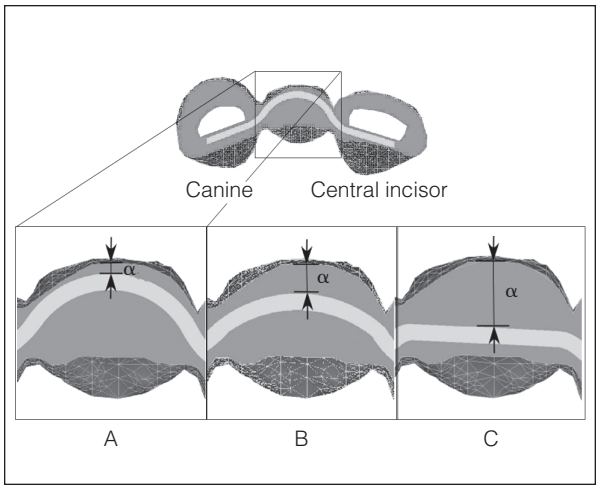

Fig 3 Design of the FRC framework (horizontal cross section). A = FRC1, α = 0.5 mm, r = 3.5 mm; B = FRC2, α = 1.5 mm, r = 5.0 mm; C = FRC3, α = 3.0 mm, r = 0.0 mm.

Table 1 Material Properties

	Young's modulus (MPa)	Poisson ratio	Shear modulus (MPa)
Hybrid composite resin	2.20×10^4	0.27	
Dentin	1.80×10^4	0.31	
Pulp	2.1	0.45	
Glass FRC			
Longitudinal	x 3.90×10^4	x 0.35	x 1.40×10^4
Transverse	y 1.20×10^4	y 0.11	y 0.54×10^4
Transverse	z 1.20×10^4	z 0.11	z 0.54×10^4

(Estenia, Kuraray Medical) was used as a veneering material. The FRC framework was constructed from unidirectional glass fiber (everStick, StickTech) with anisotropic material properties. In this FE analysis, orientation of the fiber was set as the x axis. As such, material properties of the fiber framework in the x-axis were set to have higher values (46 GPa), whereas in the y- and z-axes they were to have lower values (7 GPa), thus representing the anisotropic properties.

Hexagonal elements with 20 nodes were selected for the anisotropic fiber framework, whereas tetrahedral elements with 10 nodes represented the isotropic materials. Four different FE models were constructed in this study: C-FPD (49,450 elements; 74,028 nodes), FRC1 (50,197 elements; 79,367 nodes), FRC2 (49,884 elements; 78,678 nodes), and FRC3 (48,886 elements; 77,340 nodes). As an anisotropic material, the FRC framework offers an exceptionally high elastic modulus along the orientation of the fibers (Table 1). To exhibit the intrinsic material properties of the glass fiber, a new local coordinate system, in addition to the rectangular coordinate system, with a different point of origin needed to be established. Orientation of the fibers coincided with the major axial direction of the coordinates.

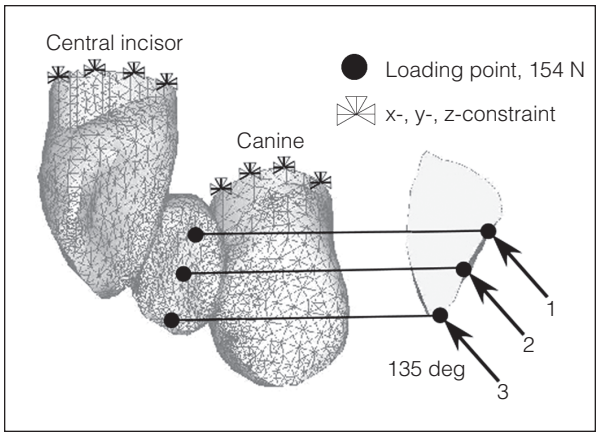

Fig 4 Boundary conditions. Condition 1: 0 mm from the incisal edge simulating edge-to-edge occlusion; condition 2 = 3 mm from the incisal edge simulating centric occlusion; condition 3 = 6 mm from the incisal edge simulating a deep overbite.

Boundary Conditions and Data Processing

Figure 4 shows the boundary and loading conditions of the FRC framework. In the present study, three different loading conditions were used to simulate edge-to-edge occlusion (1), centric occlusion (2), and a deep

© 2009 BY QUINTESSENCE PUBLISHING CO, INC. PRINTING OF THIS DOCUMENT IS RESTRICTED TO PERSONAL USE ONLY. NO PART OF THIS ARTICLE MAY BE REPRODUCED OR TRANSMITTED IN ANY FORM WITHOUT WRITTEN PERMISSION FROM THE PUBLISHER.

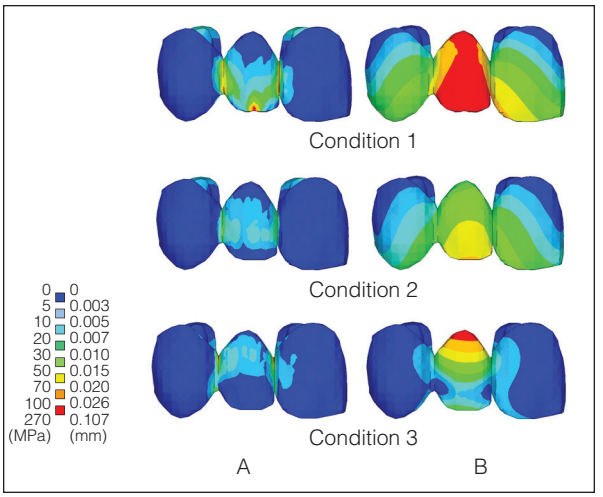

Fig 5 Maximum principal stress (A) and displacement (B) of the C-FPD (labial view). High stress concentration (red) was found in loading condition 1 and the lowest stress distribution was found in loading condition 3. Displacement was similar to maximum principal stress distribution.

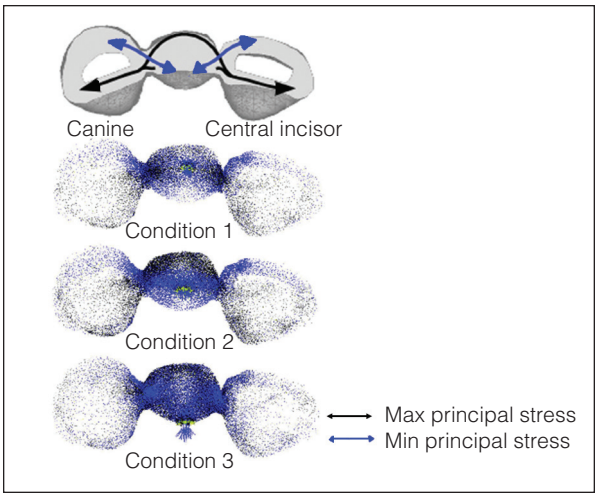

Fig 6 Vector indication of principal stress. Horizontal cross section of the C-FPD.

overbite (3), as observed during occlusion in the anterior region. A lateral load of 154 N was derived from the maximum occlusal force on healthy permanent teeth and was applied to the three different loading points of the pontic at an angle of 135 degrees from the lingual side (ie, 0 mm, 3 mm, and 6 mm from the incisal edge equidistant mesiodistally, each representing loading conditions 1, 2, and 3, respectively). The final element on the x-, y-, and z-axes of the abutment base was assumed fixed, thereby defining the boundary conditions.

FE analysis was presumed to be linear static. FE model construction and FE analysis were performed on a PC workstation (Precision Workstation 530, Dell) using ANSYS 10.0.

Results

Maximum Principal Stress and Displacement of the C-FPD

Figure 5 shows the labial view of maximum principal stress and displacement values of the C-FPD model under the three different loading conditions. Under condition 1, maximum principal stresses exceeding 100 MPa were distributed to the incisal and gingival embrasures of the mesiodistal connectors, peaking at a value of 240 MPa in the incisal embrasure of the mesial connector. Displacement exceeding 0.026 mm was observed over the entire surface of the pontic. Displacement, however, was gradually decreased from the incisal edge to the cervical side of both abutment teeth.

Under condition 2, maximum principal stresses exceeding 50 to 70 MPa were distributed across the gingival embrasure of the mesial connector, peaking at a value of 56.0 MPa. Displacement exceeding 0.020 to 0.026 mm was observed at the incisal edge of the pontic. Displacement, however, was gradually decreased from the incisal edge to the cervical side of both abutment teeth.

Under condition 3, maximum principal stresses exceeding 100 MPa were distributed to the gingival embrasure of the mesiodistal connectors, peaking at a value of 189 MPa in the gingival embrasure of the mesial connector. Displacement exceeding 0.026 mm was observed on the pontic base. Displacement, however, was gradually decreased toward the incisal edge. Concerning displacement of both abutment teeth, displacement was found to occur only on the side adjacent to the edentulous space.

Vector Indication of Principal Stress on the C-FPD

Figure 6 shows a vector indication of principal stress and an outline of principal stress direction of the C-FPD. In general, the maximum principal stress was oriented from the lingual side to the connector at the abutment tooth under all loading conditions. At the connector, the maximum principal stress was oriented from the marginal ridge of the abutment tooth (missing tooth side) to the labial side of the pontic, showing a curvature along the external form of the labial side of the pontic. At the lingual side of the pontic, the maximum principal stress was directed parallel to the external form of the pontic.

© 2009 BY QUINTESSENCE PUBLISHING CO, INC. PRINTING OF THIS DOCUMENT IS RESTRICTED TO PERSONAL USE ONLY. NO PART OF THIS ARTICLE MAY BE REPRODUCED OR TRANSMITTED IN ANY FORM WITHOUT WRITTEN PERMISSION FROM THE PUBLISHER.

Table 2 Stress Reduction and Maximum Principal Stress at the Mesial Connector

	Load condition 1		Load condition 2		Load condition 3	
	Stress (MPa)	Reduction (%)	Stress (MPa)	Reduction (%)	Stress (MPa)	Reduction (%)
C-FPD	239	–	56	–	188	–
FRC1	182	24	36	36	132	30
FRC2	189	21	37	34	135	28
FRC3	197	18	44	21	159	15

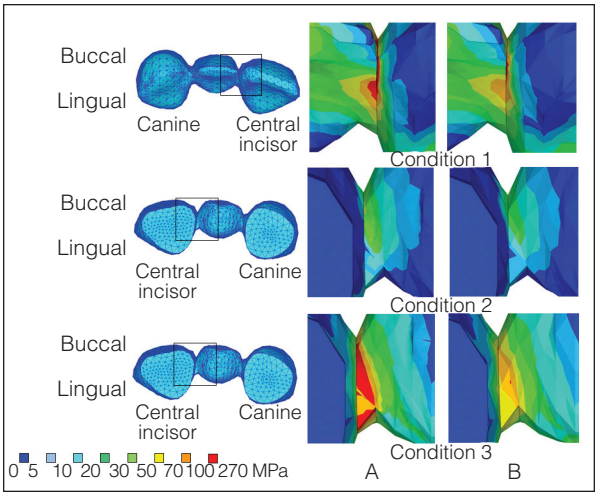

Fig 7 Maximum principal stress at the mesial connector. A = C-FPD; B = FRC1.

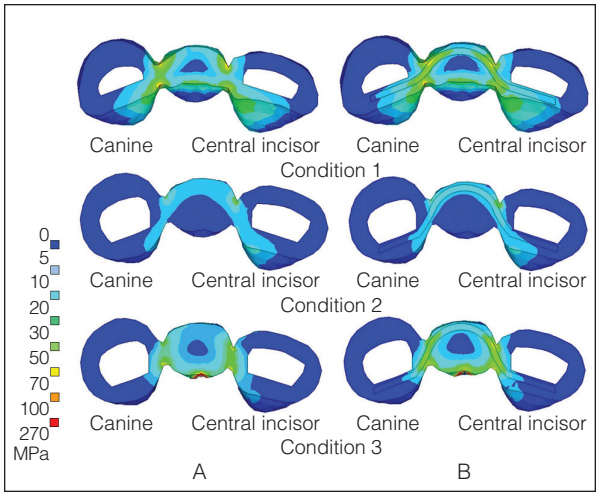

Fig 8 Maximum principal stress at the horizontal cross section. A = C-FPD; B = FRC1.

Reduction Ratio of Maximum Principal Stress on the FRC-FPD Models

Stress reduction ratio was calculated based on the difference between the maximum principal stress values of the mesial connector of the C-FPD, which detected the highest values under each loading condition (condition 1: incisal embrasure, condition 2: gingival embrasure, condition 3: gingival embrasure), and the corresponding values of the FRC-FPD models. Table 2 represents the stress reduction ratio of each model with their varying loading conditions. Stress reduction ratios of the FRC-FPD models in descending order were FRC1, FRC2, and FRC3. The highest stress reduction ratio of 36% was obtained in the combination with loading condition 2 and the FRC1 framework.

Comparison between C-FPD and FRC1 Models

Figure 7 represents the labiolingual vertical cross-sectional view of the mesial connector (recorded highest maximum principal stress value) of the C-FPD and FRC1 framework models (observed highest stress reduction ratio). Under condition 1, the mesial connector was viewed from the incisal edge, while under conditions 2 and 3, the mesial connector was viewed from the cervical edge.

Under condition 1, a high-stress area of more than 100 MPa, which had been observed in the C-FPD, was concentrated at the lowest part of the mesial connector in the FRC1. Furthermore, a 50- to 70-MPa stress area was also reduced compared to the C-FPD. Under condition 2, a 50- to 70-MPa stress area, which had been observed in the C-FPD, was not seen in the FRC1. Moreover, a 30- to 50-MPa stress area was only observed at the lowest part of the mesial connector. Under condition 3, a localized high stress area of more than 100 MPa was only observed at the pontic side of the connector in the FRC1 and the 70- to 100-MPa stress area was decreased when compared with the C-FPD.

Figure 8 represents the horizontal cross-sectional view of the stress distribution pattern generated by the three different loading conditions in the middle of the connectors of both the C-FPD and FRC1 frameworks. The C-FPD induced a high stress concentration in the outer surface of the connector, whereas the FRC1 induced the same stress in the fiber framework. The maximum principal stress generated in the resin matrix from the connector to the pontic in the C-FPD was relieved and transferred to the fiber framework in the FRC1.

© 2009 BY QUINTESSENCE PUBLISHING CO, INC. PRINTING OF THIS DOCUMENT IS RESTRICTED TO PERSONAL USE ONLY. NO PART OF THIS ARTICLE MAY BE REPRODUCED OR TRANSMITTED IN ANY FORM WITHOUT WRITTEN PERMISSION FROM THE PUBLISHER.

Concerning the displacement distribution, more than 0.026 mm of displacement, which was observed at the gingival side of the pontic in the C-FPD under condition 1, was changed to 0.020 to 0.026 mm of displacement in the FRC1. Similarly, 0.020 to 0.026 mm of displacement observed at the incisal edge of the pontic in the C-FPD under condition 2 was reduced to 0.015 to 0.020 mm of displacement in the FRC1. More than 0.026 mm of displacement, which was observed at the pontic base of the C-FPD, tended to decrease in the FRC1.

On the whole, the maximum principal stress direction pattern of the FRC-FPD models showed a similar tendency to that of the C-FPD. Once the stress direction pattern in the fiber framework of the FRC-FPD models was evaluated, the maximum principal stress was oriented uniformly along the fibers, representing a striking contrast to the C-FPD. Furthermore, the principal stress was oriented randomly at the mesiodistal connectors. This phenomenon was especially obvious in the case of the FRC1 framework.

Discussion

C-FPD Framework

In the C-FPD framework, a localized high stress concentration was observed in the connector area under all loading conditions, which might be attributable to the isotropic properties of the hybrid composite resin and the intrinsic morphology of the anterior FPD. To meet esthetic and biomechanical requirements, an anterior FPD inevitably possesses irregular and high stress concentrations around the area of the connector. Maximum principal stress distribution under condition 1 revealed that the load applied to the cutting edge had caused a bending deformation toward the labial side, which further induced the twisting force toward the labial side rotating around the lower embrasure of the mesiodistal connectors. High stress concentration around the upper embrasure of the connector was mainly generated by two factors: the large displacement of the pontic and the combined effects of both the bending and twisting forces.[27–29] Under condition 2, a load applied at the center of the lingual surface (3 mm from the incisal edge) induced less twisting force against the FPD, resulting in small displacement and lower stress values. Under condition 3, a large displacement was observed around the pontic base, which was mainly induced by the turning behavior of the pontic when it rotated around the upper embrasure of the mesiodistal connectors.

High stress concentrations around the lower embrasure of the connector might be induced by the twisting behavior with the connector as a fixed point. Maximum principal stress direction patterns at the pontic of the C-FPD resulting from the compressive stress generated in the lingual side and tensile stress in the labial side showed a curvature along the external form of the labial side. Maximum principal stress direction patterns from the abutment tooth to the connector, due to the shear force generated from the lingual marginal ridge to the labial side of the pontic, showed a curvature along the lingual side of the abutment tooth and the labial side of the pontic. These FE test results revealed that critical factors such as FPD morphology, loading points, and loading direction greatly affect the stress direction pattern.[30–32]

FRC-FPD Frameworks

The stress reduction ratio of the maximum principal stress obtained from the differences between the C-FPD and FRC-FPD models (FRC1, FRC2, and FRC3) showed that the FRC1 model obtained the highest stress reduction ratio under all loading conditions. The results suggested that the fiber framework, which had been placed within a high stress distribution area of the labial side, effectively bore more tensile stress. Concerning FRC2 and FRC3, inappropriate positioning of the fiber framework placement only affected the stress distribution pattern and not the stress reduction ratio, indicating a small reduction ratio. When investigating the influence of the fiber framework on displacement, it was found to be reduced only at the pontic of the FRC1. When evaluating the displacement distribution pattern of the abutment teeth and connectors, no significant differences were found among the C-FPD and models reinforced with a fiber framework. As for the direction of maximum principal stress on the whole, no significant differences were found among the C-FPD and models reinforced with a fiber framework. At the fiber framework, however, maximum principal stress tended to be directed along the orientation of the fiber, and the direction of the fiber framework and maximum principal stress partially coincided with one another. This demonstrated a striking contrast to the C-FPD model, of which the principal stress was oriented randomly at the mesiodistal connectors.

Optimum Design of the Fiber Framework

Fiberglass is suitable for a wide range of clinical applications,[33] including reinforcement for a denture base,[34] orthodontic appliance,[35,36] or core construction.[37] For prostheses to function successfully for a long time in a rigorous oral environment, it is critical to make the most of the anisotropic nature of the fiber framework (ie, having an exceptionally high Young's and elastic modulus along the orientation of the fibers).

© 2009 BY QUINTESSENCE PUBLISHING CO, INC. PRINTING OF THIS DOCUMENT IS RESTRICTED TO PERSONAL USE ONLY. NO PART OF THIS ARTICLE MAY BE REPRODUCED OR TRANSMITTED IN ANY FORM WITHOUT WRITTEN PERMISSION FROM THE PUBLISHER.

Continuous unidirectional glass fiber is used as the reinforcing framework in an FPD. Obtaining the maximum reinforcement effects of the fiber framework and avoiding high irregular stress concentration are very important when designing an FPD. The present study demonstrated that the maximum reinforcement benefit was achieved with the FRC1 under all loading conditions, indicating an approximately 36% maximum principal stress reduction compared with the C-FPD. The results of this study revealed that fiber frameworks possess excellent reinforcement benefits.

Esthetic treatment for the anterior tooth region often requires use of materials with varying color shades. Extensive space is needed to place different combinations of composite shades, especially in the incisal edge region of anterior teeth. In order to achieve good esthetics when working with anterior teeth, a labial space of 0.5 mm is considered to be the minimum for layered veneering composites with different color shades.

However, the middle part at the labial side of the pontic in the anterior tooth area does not require the use of more than dentin and enamel veneering composite shades on top of the FRC1 framework, since an FRC framework can use EG fiber (Kuraray Medical) with a dentin-colored shading or everStick with a translucent shading. FRC materials are practical in achieving the natural tooth color with both the layering and staining techniques.

Fiber-reinforced anterior FPDs were investigated from a biomechanical and structural point of view and it was found that the optimal fiber reinforcement effect is achieved with a curved FRC extending from the lingual side of both abutment teeth to the labial side of the pontic base.

Conclusions

Within the limitations of this in vitro study, the following conclusions can be drawn:

1. Localized high stress concentration was observed around the connectors under all loading conditions.
2. In all FRC–FPD models, the fiber framework bore the stress generated, showing the stress-bearing capacity of the FRC framework. The highest stress reduction ratio was obtained with a curved FRC extending from the lingual side of both abutment teeth to the labial side of the pontic base.
3. Fiber reinforcement also enabled the reduction of the quantified displacement.

References

1. Vallittu PK. The effect of glass fiber reinforcement on the fracture resistance of a provisional fixed partial denture. J Prosthet Dent 1998;79:125–130.
2. Vallittu PK, Sevelius C. Resin-bonded, glass fiber-reinforced composite fixed partial dentures: A clinical study. J Prosthet Dent 2000;84:413–418.
3. Bae JM, Kim KN, Hattori M, et al. The flexural properties of fiber-reinforced composite with light-polymerized polymer matrix. Int J Prosthodont 2001;14:33–39.
4. Lastumäki TM, Kallio TT, Vallittu PK. The bond strength of light-curing composite resin to finally polymerized and aged glass fiber-reinforced composite substrate. Biomaterials 2002;23: 4533–4539.
5. Handa I, Shinya A, Gomi H, Sailynoja ES. Bending strength of fiber reinforced posterior hybrid resin material [in Japanese]. J J Dent Mater 2003;22:171–180.
6. Sailynoja ES , Shinya A, Gomi H, Ishii Y. The effect of immersion temperature on the flexural strength of a pre-coated fiber reinforced composite resin. Prosthodont Res Pract 2003;2:1–10.
7. Nakamura T, Waki T, Kinuta S, Tanaka H. Strength and elastic modulus of fiber-reinforced composites used for fabricating FPDs. Int J Prosthodont 2003; 16:549–553.
8. Drummond JL, Bapna MS. Static and cyclic loading of fiber-reinforced dental resin. Dent Mater 2003;19:226–231.
9. Tezvergil A, Lassila LVJ, Vallittu PK. Composite-composite repair bond strength: Effect of adhesion primers. J Dent 2003;31:521–525.
10. Tezvergil A, Lassila LVJ, Vallittu PK. Strength of adhesive-bonded fiber-reinforced composites to enamel and dentin substrates. J Adhes Dent 2003;5:301–311.
11. Vallittu PK. Survival rates of resin-bonded, glass fiber-reinforced composite fixed partial dentures with a mean follow-up of 42 months: A pilot study. J Prosthet Dent 2004;91:241–246.
12. Säilynoja ES, Shinya A, Koskinen MK, et al. Heat curing of UTMA-based hybrid resin: Effects on the degree of conversion and cytotoxicity. Odontology 2004;92:27–35.
13. Shimizu K, Shin-ya A, Gomi H, Nakasone Y. Fatigue properties of hybrid resin with glass fiber reinforcement—The influence of cyclic loading, glass fiber reinforcement and test environments [in Japanese]. J J Dent Mater 2004;23:294–305.
14. Bae JM, Kim KN, Hattori M, et al. Fatigue strengths of particulate filler composites reinforced with fibers. Dent Mater J 2004;23: 166–174.
15. Lassila LVJ, Tezvergil A, Lahdenperä M, et al. Evaluation of some properties of two fiber-reinforced composite materials. Acta Odontol Scand 2005;63:196–204.
16. Nakamura T, Ohyama T, Waki T, et al. Finite element analysis of fiber-reinforced fixed partial dentures. Dent Mater J 2005;24: 275–279.
17. Fennis WM, Tezvergil A, Kuijs RH, et al. In vitro fracture resistance of fiber reinforced cusp-replacing composite restorations. Dent Mater 2005;21:565–572.
18. Waki T, Nakamura T, Nakamura T, Kinuta S, Wakabayashi K, Yatani H. Fracture resistance of inlay-retained fixed partial dentures reinforced with fiber-reinforced composite. Dent Mater J 2006;25:1–6.
19. Shinya A, Matsuda T, Shinya A, Nakasone Y. Hybrid resin fixed partial dentures reinforced with glass fiber—Optimum posterior fiber frame design with finite element analysis [in Japanese]. J J Dent Mater 2004;23:183–192.
20. Ootaki M, Shinya A, Gomi H, Shinya A, Nakasone Y. Optimum design for fixed partial dentures made of hybrid resin with glass fiber reinforcement by finite element analysis: Effect of vertical reinforced thickness on fiber frame. Dent Mater J 2007;26:280–289.

© 2009 BY QUINTESSENCE PUBLISHING CO, INC. PRINTING OF THIS DOCUMENT IS RESTRICTED TO PERSONAL USE ONLY. NO PART OF THIS ARTICLE MAY BE REPRODUCED OR TRANSMITTED IN ANY FORM WITHOUT WRITTEN PERMISSION FROM THE PUBLISHER.

21. Fujita T. Textbook of Dental Anatomy, ed 22. Tokyo: Kanehara, 1995:75–104.
22. el-Ebrashi MK, Craig RG, Peyton FA. Experimental stress analysis of dental restorations. VII: Structural design and stress analysis of fixed partial dentures. J Prosthet Dent 1970;23:177–186.
23. Krejci I, Reich T, Lutz F, Albertoni M. An in vitro test procedure for evaluating dental restoration systems. 1. A computer-controlled mastication simulator [in German]. Schweiz Monatsschr Zahnmed 1990;100:953–960.
24. Belvedere PC. Single-sitting, fiber-reinforced fixed bridges for the missing lateral or central incisors in adolescent patients. Dent Clin North Am 1998;42:665–682.
25. Göhring TN, Mörmann WH, Lutz F. Clinical and scanning electron microscopic evaluation of fiber-reinforced inlay fixed partial dentures: Preliminary results after one year. J Prosthet Dent 1999;82: 662–668.
26. Rudo DN, Karbhari VM. Physical behaviors of fiber reinforcement as applied to tooth stabilization. Dent Clin North Am 1999;43:7–35.
27. Freilich MA, Meiers JC, Duncan JP, Goldberg AJ. Fiber-reinforced composites in clinical dentistry. Chicago: Quintessence, 2000:1–21.
28. Rosentritt M, Behr M, Lang R, Handel G. Experimental design of FPD made of all-ceramics and fiber-reinforced composite. Dent Mater 2000;16:159–165.
29. Magne P, Perakis N, Belser UC, Krejci I. Stress distribution of inlay-anchored adhesive fixed partial dentures: A finite element analysis of the influence of restorative materials and abutment preparation design. J Prosthet Dent 2002;87:516–527.
30. Yang HS, Lang LA, Felton DA. Finite element analysis on the effect of splinting in fixed partial dentures. J Prosthet Dent 1999;81: 721–728.
31. Kelly JR, Tesk JA, Sorensen JA. Failure of all-ceramic fixed partial dentures in vitro and in vivo: Analysis and modeling. J Dent Res 1995;74:1253–1258.
32. Meiers JC, Kazemi RB, Donadio M. The influence of fiber reinforcement of composites on shear bond strengths to enamel. J Prosthet Dent 2003;89:388–393.
33. Lassila LVJ, Nohrström T, Vallittu PK. The influence of short-term water storage on the flexural properties of unidirectional glass fiber-reinforced composites. Biomaterials 2002;23:2221–2229.
34. Nakamura M, Takahashi H, Hayakawa I. Reinforcement of denture base resin with short-rod glass fiber. Dent Mater J 2007;26: 733–738.
35. Cacciafesta V, Sfondrini MF, Norcini A, Macchi A. Fiber-reinforced composites in lingual orthodontics. J Clin Orthod 2005;39: 710–714.
36. Brauchli LM, Wiedmer C, Wichelhaus A. A light-focusing tool for bonding fiber-reinforced composite retainers. J Clin Orthod 2006;40:359–360.
37. Lassila LVJ, Tanner J, Le Bell AM, Narva K, Vallittu PK. Flexural properties of fiber reinforced root canal posts. Dent Mater 2004;20: 29–36.

Literature Abstract

Effects of implant geometry and surface treatment on osseointegration after functional loading: A dog study

The aim of this paper is to evaluate the effects of changing the pitch height and surface characteristics on osseointegration after functional loading by radiographic and histomorphometric analyses. External hexagon type implants were fabricated by machining commercially pure grade II titanium. Group 1 was the control consisting of Brånemark implants, Group 2 had a 0.5-mm screw pitch height and a machined surface, and Group 3 had a 0.5-mm screw pitch height and was thermally oxidized to create a roughened surface. The surface roughness of each implant was measured using an interferometer. Four beagle dogs were used in this animal study. Six implants were placed into each dog, three in the left and right mandibles randomly. A 3-month healing period was allowed and after which, a second stage surgery was performed to expose the implants. One month later, standard abutments were torqued onto the implants and fixed partial dentures were made from type IV gold. Radiographic and periodontal assessments were made at the point of insertion and at 6- and 12-month intervals, after which the animals were sacrificed for histomorphometirc analysis. Samples were fixed, embedded in resin, and sectioned and stained before viewing under light microscopy. The bone to implant contact was calculated from these sections. The results showed that Group 2 was significantly rougher than Groups 1 or 3 and radiographic bone loss was less in the experimental compared with the control groups. There did not seem to be any difference in the periodontal assessment across groups but histomorphometric analysis showed a mean BIC of 83.7% for Group 3 as compared with 74.4% and 75% for Groups 1 and 2, respectively. The conclusion was that alterations in the pitch height and surface treatment induced enhanced bone response following functional loading, reducing crestal resorption and improving bone healing. However, mechanisms of surface modification requires further study.

Chung SH, Heo SJ, Koak JY, et al. *J Oral Rehabil* 2008;35:229–236. **References:** 24. **Reprints:** S. K. Kim, Department of Prosthodontics and Dental Research Institute, College of Dentistry, Seoul National University, 28–1, Yeungun-Dong, Chongno-Gu, 110–749 *Seoul, Korea—Y. L. Seetoh, Singapore*

© 2009 BY QUINTESSENCE PUBLISHING CO, INC. PRINTING OF THIS DOCUMENT IS RESTRICTED TO PERSONAL USE ONLY. NO PART OF THIS ARTICLE MAY BE REPRODUCED OR TRANSMITTED IN ANY FORM WITHOUT WRITTEN PERMISSION FROM THE PUBLISHER.

Copyright of International Journal of Prosthodontics is the property of Quintessence Publishing Company Inc. and its content may not be copied or emailed to multiple sites or posted to a listserv without the copyright holder's express written permission. However, users may print, download, or email articles for individual use.